Application of the Ffowcs Williams/Hawkings equation to two-dimensional problems

By Y. P. GUO

The Boeing Company, Mail Code C078-0420, 2401 E. Wardlow Road,
Long Beach CA 90807, USA

This paper discusses the application of the Ffowcs Williams/Hawkings equation to two-dimensional problems. A two-dimensional version of this equation is derived, which not only provides a very efficient way for numerical implementation, but also reveals explicitly the features of the source mechanisms and the characteristics of the far-field noise associated with two-dimensional problems. It is shown that the sources can be interpreted, similarly to those in three-dimensional spaces, as quadrupoles from turbulent flows, dipoles due to surface pressure fluctuations on the bodies in the flow and monopoles from non-vanishing normal accelerations of the body surfaces. The cylindrical spreading of the two-dimensional waves and their far-field directivity become apparent in this new version. It also explicitly brings out the functional dependence of the radiated sound on parameters such as the flow Mach number and the Doppler factor due to source motions. This dependence is shown to be quite different from those in three-dimensional problems. The two-dimensional version is numerically very efficient because the domains of the integration are reduced by one from the three-dimensional version. The quadrupole integrals are now in a planar domain and the dipole and monopole integrals are along the contours of the two-dimensional bodies. The calculations of the retarded-time interpolation of the integrands, a time-consuming but necessary step in the three-dimensional version, are completely avoided by making use of fast Fourier transform. To demonstrate the application of this, a vortex/airfoil interaction problem is discussed, which has many practical applications and involves important issues such as vortex shedding from the trailing edge.

1. Introduction

Many acoustic problems in engineering applications can be approximated as two-dimensional, sound generation by leading-edge slats in aircraft high-lift systems (Guo 1997) and local flows in flap side edge regions (Hardin 1980; Sen 1996; Guo 1999) being just two examples associated with aircraft noise. This kind of approximation can greatly simplify the task of acoustic modelling, by reducing computational efforts by orders of magnitude, both in the near-field and the far-field calculations. For the latter, a widely used approach is the Ffowcs Williams/Hawkings equation (1969), which is cast for three-dimensional geometry with the results expressed in terms of volume and surface integrals. In principle, this result can be applied to both three- and two-dimensional problems. When it is applied to two-dimensional problems, the source domains are treated as three-dimensional, but with identical source distributions in one direction to simulate the two-dimensional nature of the

applications. This is not only inefficient, but also prone to failure. It is inefficient because the integrations have to be carried out over a large range in the direction in which the sources are invariant. It is prone to failure because the invariance of sources in this direction makes the convergence of the integrals critically depend on the retarded-time variations of the integrands. Furthermore, the functional dependence of the far-field sound on parameters such as flow Mach numbers, the Doppler factor and the propagation distance, which may be quite different from those in three-dimensional problems, are all buried in the numerical integrations, making the understanding of the source mechanisms difficult. This makes it desirable to develop an explicitly two-dimensional version of the Ffowcs Williams/Hawkings equation, and it is the topic of this paper.

The derivations of the Ffowcs Williams/Hawkings equation in two-dimensional planes are different from those in three-dimensional spaces. This is essential because of the different behaviour of the Green functions of the wave equation in the two cases. In a three-dimensional space, the Green function is simply a Dirac delta function, implying that a pulse generated by a source would propagate away from the source as a pulse with its shape remaining unchanged and its amplitude decaying according to the law of spherical spreading. In a two-dimensional plane, however, a pulse from the source would propagate away from it in the form of a wavefront followed by a long tail. The shape of the signal in the far field is very different from that at the source and its amplitude decay follows the cylindrical spreading. This behaviour clearly manifests itself in the mathematical form of the Green function, which is given by a Heaviside function with an amplitude that becomes singular at the wavefront and decays slowly in the tail following the wavefront (e.g. Crighton 1975). This particular form of the two-dimensional Green function makes it difficult to derive the Ffowcs Williams/Hawkings equation in the form of retarded-time integrals, as is done in three-dimensional spaces by making use of the Dirac delta function. To overcome this difficulty, we will use the two-dimensional Green function in the form of its Fourier integral representation. This, after some mathematical manipulations, enables us to reduce the result to a form very similar to that in three-dimensional problems. In this two-dimensional version, we will show that the noise sources are interpreted in the same way as those in three dimensions. The sound is now given by an integral over a planar domain in which turbulence sources have non-zero strengths, together with two contour integrals over the outlines of the two-dimensional bodies in the flow with the integrands respectively determined by the unsteady pressures and normal accelerations on the bodies. This is clearly the same interpretation of the noise source mechanisms as for three-dimensional flows, but with the source domains reduced by one dimension.

Clearly, this two-dimensional version requires much less computational effort than that required by applying the three-dimensional version to two-dimensional problems, because of the reduction in integration domains. For example, the dipole term that is given by the unsteady pressures on the body surface can now be computed along a contour, instead of over a surface, which differ in computational time by orders of magnitude. The computational effort is further reduced by completely avoiding the retarded-time calculation so that no interpolation is needed in the calculation of the integrands. This is a time-consuming but necessary step in the three-dimensional version because the sampling at emission time, often from near-field computations, does not usually coincide with the sampling at receiving time. Thus, interpolations have to be used to find the values of the integrands at the retarded time for the integration. This is avoided in the two-dimensional version by making use of Fourier

transforms, which does not add any noticeable computation effort because numerical fast Fourier transformation is very efficient.

We will show that the two-dimensional version of the Ffowcs Williams/Hawkings equation explicitly brings out the characteristics of the far-field noise unique to two-dimensional problems. The propagation of the waves will be characterized explicitly by cylindrical spreading with two-dimensional far-field directivities. The amplitudes of the waves decay according to the inverse of the square root of the propagation distance. The dependence of the far-field radiation on the flow Mach number is also explicitly brought out: the acoustic pressure scales on power laws of the flow Mach number with power indices given by $(2n + 3)/2$, where $n = 0, 1, 2$ respectively for monopoles, dipoles and quadrupoles. These are different from those for three-dimensional sources, and have been previously discussed (e.g. Ffowcs Williams 1969; Crighton 1975). It will be shown that the sound fields from the three different types of sources experience different amplitude amplification due to the Doppler effect when the sources are in motion. The amplification is in terms of power laws of the Doppler factor, with power indices given by $(2n + 1)/2$, which again is again quite different from those for three-dimensional sources.

The explicit functional dependence of the radiated sound on flow parameters can help understand and interpret better source mechanisms in practical applications. A typical example is the noise from leading-edge slats of aircraft high-lift systems. Airframe noise intensity has long been observed to scale on the flow Mach number according to the 5th power law in the middle frequency domain centred at about 1000 Hz. This coincides with the prediction of sound scattered from turbulent flows by a sharp edge (Ffowcs Williams & Hall 1970). Thus, this component of airframe noise has been attributed to the sharp trailing edges of the wings (e.g. Bauer & Munson 1978; Fink 1979). While this may explain airframe noise from clean wing configurations when the high-lift systems are not deployed (Crighton 1991), it is not supported by recent test data (Sen *et al.* 1997; Guo *et al.* 1999). The data show that airframe noise in the middle frequency domain is dominantly generated in the slat region, probably due to flow separation in the cove region of the slats (Guo 1997), instead of the trailing edges of the wings. In this case, the 5th power law is more likely to be associated with the two-dimensional nature of the sources, rather than the sharp-edge scattering. The sharp edges of the slats, namely their cusps and trailing edges, are in a relatively 'clean' flow without intense turbulence fluctuations. Thus, the scattering, if any, would be relatively weak because according to the theory by Ffowcs Williams & Hall (1970), strong scattering occurs only when intense turbulence fluctuations exist in a region close to the sharp edges within a typical wavelength. Also important to note is that the 5th power law from sharp-edge scattering results from the assumption of potential flow at the edge where the flow becomes singular. If the flow is regular at the edge as commonly implied when the Kutta condition is applied, the scattered noise would not follow the 5th power law, which is also explicitly pointed out in Ffowcs Williams & Hall (1970). All this indicates that the experimentally observed 5th power law of the middle frequency component in airframe noise may be more satisfactorily understood by the two-dimensional nature of the sources associated with the slats, rather than the sharp-edge scattering mechanism.

To illustrate the application of the two-dimensional version of the Ffowcs Williams/Hawkings equation, we will discuss a vortex/airfoil interaction problem where a concentrated vortex is incident upon a two-dimensional airfoil in a uniform mean flow. In response to the fluctuations caused by the incident vortex, vorticity is shed from the trailing edge of the airfoil, leading to further fluctuations. The problem is

simple enough to be analysed easily, but yet has practical applications (e.g. Howe 1978; Brooks & Hodgson 1981; Amiet 1976). It also involves the issue of the Kutta condition at sharp edges in acoustic applications, a topic that has a long history of research and discussion (e.g. Howe 1976; Crighton 1981, 1985; Amiet 1990). For acoustic modelling, it is now well-known that the absence of the Kutta condition over-predicts the radiated noise (Howe 1976) and in general, the Kutta condition applies provided that the Strouhal number is not larger than the flow Reynolds number to the power of $\frac{1}{4}$ (Crighton 1991). This is almost always the case for aircraft applications where the airfoil may represent individual components of the aircraft high-lift systems or individual blades of rotors. To impose the Kutta condition, we will follow a nonlinear flow separation model, based on the Brown & Michael (1954) equation and recently improved by Howe (1996). In this model, flow separation is accounted for by unsteady vorticity production at the sharp edge. The shed vorticity is in the form of a vortex sheet, connecting the edge with a vortex core that accumulates the shed vorticity through the vortex sheet. Under the joint effects of local convecting flows and the flow induced by the vortical field, the vortex core experiences fully nonlinear motions and unsteady strength fluctuations, both of them being potential noise sources according to the theory of vortex sound (Powell 1964; Howe 1975). With this model, the near-field flow will be solved, including unsteady pressure fluctuations on the airfoil surface. The surface pressures will then be used to calculate the far-field noise by implementing the two-dimensional version of the Ffowcs Williams/Hawkings equation.

2. The Ffowcs Williams/Hawkings equation in two-dimensional format

We start with the generalized wave equation derived by Ffowcs Williams & Hawkings (1969) that combines the equations governing the conservation laws of unsteady flows with a wave equation driven by sources due to flow fluctuations, as originated by Lighthill (1952). In two-dimensional notation, this equation reads

$$\left(\frac{1}{c^2} \frac{\partial^2}{\partial t^2} - \frac{\partial^2}{\partial x_\alpha^2} \right) H(f) \, p(x_\alpha, t) = Q(x_\alpha, t), \tag{2.1}$$

where the flow-generated sound is represented by the fluctuating pressure $p(x_\alpha, t)$, t being time and $x_\alpha (\alpha = 1, 2)$ being the coordinates in two dimensions. The flow is in the region outside any bodies, whose surfaces are given by the equation,

$$f(x_\alpha, t) = 0, \tag{2.2}$$

so that the Heaviside function $H(f)$ in (2.1) is equal to unity and zero respectively outside and inside the bodies. A schematic illustration of the problem, together with the coordinate systems, is given in figure 1. Away from the flow region, the only disturbances are assumed to be acoustic, characterized by the wave operator on the left-hand side of (2.1) with constant sound speed c. The wave operator is driven by sources collectively denoted by Q with the definition

$$Q(x_\alpha, t) = \frac{\partial^2 H(f) T_{\alpha\beta}}{\partial x_\alpha \partial x_\beta} - \frac{\partial}{\partial x_\alpha} \left(\frac{\partial H(f)}{\partial x_\beta} P_{\alpha\beta} \right) + \frac{\partial}{\partial t} \left(\frac{\partial H(f)}{\partial x_\alpha} \rho_0 u_\alpha \right). \tag{2.3}$$

Here, ρ_0 is the constant mean density and the subscripts α and β are used to emphasize the two-dimensional nature of the problem with $\alpha, \beta = 1, 2$. As in the three-dimensional case, the sources are given by three terms: the Reynolds stress tensor $T_{\alpha\beta}$, the surface stress $P_{\alpha\beta}$ and the velocity of the bodies u_α. The last two

terms can be identified as surface quantities because the derivative of the Heaviside functions yields

$$\frac{\partial H(f)}{\partial x_\alpha} = \delta(f)\frac{\partial f}{\partial x_\alpha}, \tag{2.4}$$

where δ is the Dirac delta function. Because of the Heaviside function, equation (2.1) is valid in the entire x_α-plane so that it can be solved by making use of the Green theorem. Symbolically, the solution is simply

$$p(x_\alpha, t) = \int_{y_\alpha} \int_\tau Q(y_\alpha, \tau)G(x_\alpha - y_\alpha, t - \tau)\,d^2y_\alpha\,d\tau, \tag{2.5}$$

with G denoting the free-space Green function and the integrations performed over the entire source plane y_α and source time τ. For two-dimensional problems, the Green function can be conveniently expressed in terms of its Fourier transform representation (e.g. Crighton 1975),

$$G = \frac{i}{8\pi} \int_\omega H_0^{(1)}(kR)e^{-i\omega(t-\tau)}\,d\omega. \tag{2.6}$$

Here, $H_0^{(1)}$ is the zeroth-order Hankel function of first kind that has outgoing wave behaviour when its argument kR is much larger than unity, where $k = \omega/c$ is the acoustic wavenumber, ω being the angular frequency, and $R = |x_\alpha - y_\alpha|$ is the distance between source and receiver. When (2.3) and (2.6) are substituted into the solution (2.5), the integrations in source-plane and time can be carried out in part so that the differentiations are transferred onto the Hankel functions. This leads to

$$p(x_\alpha, t) = \frac{i}{8\pi} \int_\omega \int_{y_\alpha} \int_\tau \left\{ H(f)T_{\alpha\beta}\frac{\partial H_0^{(1)}(kR)}{\partial y_\alpha\,\partial y_\beta} \right.$$
$$\left. + P_{\alpha\beta}\frac{\partial H(f)}{\partial y_\beta}\frac{\partial H_0^{(1)}(kR)}{\partial y_\alpha} + \rho_0 A_\alpha H_0^{(1)}(kR)\frac{\partial H(f)}{\partial y_\alpha} \right\} e^{-i\omega(t-\tau)}\,d\omega\,d^2y_\alpha\,d\tau. \tag{2.7}$$

Here, to facilitate the physical interpretation of the sources, we have introduced the acceleration of the body surfaces A_α, defined by

$$A_\alpha = \partial u_\alpha/\partial\tau. \tag{2.8}$$

The two terms on the second line of (2.7) can now be simplified further by making used of (2.4). To do this, the coordinate system y_α for the spatial integration is changed to η_α which is fixed on the moving body so that the function f defined in (2.2) is independent of time in this new coordinate system. The change of coordinate systems can be expressed as

$$y_\alpha = \eta_\alpha + \int^\tau U_\alpha(\tau')\,d\tau', \tag{2.9}$$

where U_α is the velocity of the moving body in the α-direction. Note also that the result before the ω-integration in (2.7) is precisely the Fourier transform of $p(x_\alpha, t)$ with respect to t, namely its spectrum. This, together with the use of (2.2) to reduce the planar integration to contour integration, leads to

$$\tilde{p}(x_\alpha, \omega) = \frac{i}{4} \int_{\eta_\alpha} \int_\tau T_{\alpha\beta}\frac{\partial^2 H_0^{(1)}(kR)}{\partial\eta_\alpha\,\partial\eta_\beta}e^{i\omega\tau}\,d\tau\,d^2\eta_\alpha$$
$$+ \frac{i}{4} \int_S \int_\tau \left(P_{\alpha\beta}\,n_\beta\frac{\partial H_0^{(1)}(kR)}{\partial\eta_\alpha} + \rho_0 A_\alpha n_\alpha H_0^{(1)}(kR) \right) e^{i\omega\tau}\,d\tau\,ds, \tag{2.10}$$
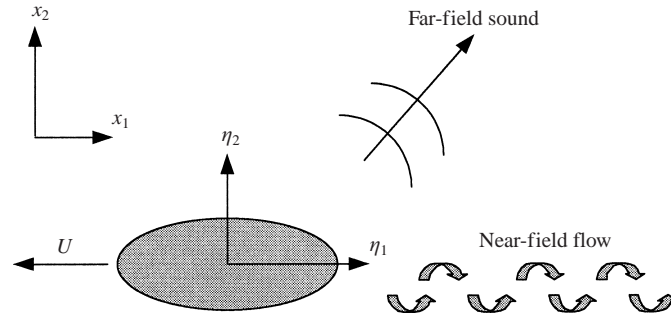
FIGURE 1. Schematic of the problem of sound generation by a two-dimensional body moving at velocity U. The coordinate system (η_1, η_2) moves with the body and the fixed coordinate system is (x_1, x_2).

where n_α is the α-component of the outward unit normal for the body surface and the title denotes quantities in the Fourier transform domain, defined by

$$\tilde{p}(x_\alpha, \omega) = \int_t p(x_\alpha, t) e^{i\omega t}\, \mathrm{d}t \quad \text{and} \quad p(x_\alpha, t) = \frac{1}{2\pi} \int_\omega \tilde{p}(x_\alpha, \omega) e^{-i\omega t}\, \mathrm{d}\omega. \tag{2.11}$$

The first line in (2.10) is a planar integral with the domain of integration in the flow where the unsteady quantity $T_{\alpha\beta}$ is non-zero. The second line is basically a contour integral, along the outline of the two-dimensional body, denoted by S.

This is clearly very similar to the three-dimensional version derived by Ffowcs Williams & Hawkings (1969), in that the sources are interpreted as quadrupoles, dipoles and monopoles. The integration domains for the integrals, however, are reduced, respectively from spaces and surfaces to planes and contours. Another difference between the two cases is that the three-dimensional version is in terms of retarded-time integrals while (2.10) does not involve any retarded-time calculation, but with its integrands essentially expressed in terms of Fourier transforms (which will become even more apparent in the next section). It is known that the retarded-time integrals in the three-dimensional version results from the three-dimensional Green function in the form of the Dirac delta function. That feature is absent in the two-dimensional result (2.10) because the Green function in this case cannot be expressed as simply as a Dirac delta function. The space–time Green function can be derived from (2.6) as (e.g. Ffowcs Williams 1969; Crighton 1975)

$$G(x_\alpha - y_\alpha, t - \tau) = \frac{c}{2\pi} \frac{H\left[c(t - \tau) - |x_\alpha - y_\alpha|\right]}{[c^2(t - \tau)^2 - |x_\alpha - y_\alpha|^2]^{1/2}}. \tag{2.12}$$

This difference in the mathematical forms reflects a fundamental difference in the behaviour of the waves in the two cases. For a three-dimensional source, a signal generated by a source would propagate away from it and reach an observer at the retarded time with the shape of the signal unchanged, precisely the behaviour of the Dirac delta function. For a two-dimensional source, however, (2.12) shows that the signal would reach the observer with a singular wavefront followed by a long tail. The signal is spread in time with decaying amplitude in the tail. Thus, the observer receives the waves at all time after the retarded time.

When numerically implementing (2.10), the derivatives of the Hankel functions can be simplified by making use of the recursive relations between Hankel functions. In

particular, we have

$$\frac{\partial^2 H_0^{(1)}(kR)}{\partial \eta_\alpha \partial \eta_\beta} = \frac{k(x_\alpha - y_\alpha)(x_\beta - y_\beta)}{R^3}(2H_1^{(1)}(kR) - kRH_0^{(1)}(kR)), \tag{2.13}$$

and

$$\frac{\partial H_0^{(1)}(kR)}{\partial \eta_\alpha} = \frac{k(x_\alpha - y_\alpha)}{R}H_1^{(1)}(kR), \tag{2.14}$$

where y_α is given in terms of η_α by (2.8) and $H_1^{(1)}$ is the first-order Hankel function of the first kind. These results are also useful when discussing the far-field characteristics, as is done in the next section.

3. Far-field characteristics

The far-field behaviour of the radiated sound in two-dimensional problems can be studied using (2.10) with the usual far-field assumption that the observation point is far away from the sources:

$$|x_\alpha| \gg |y_\alpha| \quad \text{and} \quad kR \gg 1. \tag{3.1}$$

Under these conditions, the Hankel functions in (2.13) and (2.14) have the asymptotic form

$$\left\{ \begin{array}{c} H_0^{(1)}(kR) \\ H_1^{(1)}(kR) \end{array} \right\} = \left\{ \begin{array}{c} 1 \\ -i \end{array} \right\} \left(\frac{2}{\pi kR} \right)^{1/2} e^{i(kR - \pi/4)}. \tag{3.2}$$

Further simplification can be made by noting that $1/R$ reduces to $1/|x_\alpha|$ in the far field and the phase function in (3.2) can be approximated by

$$\exp(ikR) = \exp(ik|x_\alpha| - iky_\alpha \hat{x}_\alpha), \tag{3.3}$$

which comes from expanding kR at large $|x_\alpha|$ and denoting

$$\hat{x}_\alpha = x_\alpha/|x_\alpha|. \tag{3.4}$$

With this, the three terms involving the Hankel functions in (2.10) reduce to

$$\left\{ \begin{array}{c} \partial^2 H_0^{(1)}(kR)/\partial \eta_\alpha \partial \eta_\beta \\ \partial H_0^{(1)}(kR)/\partial \eta_\alpha \\ H_0^{(1)}(kR) \end{array} \right\} = \left\{ \begin{array}{c} -k^2 \hat{x}_\alpha \hat{x}_\beta \\ -ik\hat{x}_\alpha \\ 1 \end{array} \right\} \left(\frac{2}{i\pi k|x_\alpha|} \right)^{1/2} e^{ik|x_\alpha| - iky_\alpha \hat{x}_\alpha}. \tag{3.5}$$

By substituting this into (2.10), we have the far-field sound pressure in the form

$$\tilde{p}(x_\alpha, \omega) = e^{ik|x_\alpha|} \left(\frac{1}{8i\pi k|x_\alpha|} \right)^{1/2} \left\{ -ik^2 \hat{x}_\alpha \hat{x}_\beta \int_{\eta_\alpha} \tilde{T}_{\alpha\beta}(\eta_\alpha, \omega_D) e^{-ik\eta_\alpha \hat{x}_\alpha} \, d^2 \eta_\alpha \right.$$

$$\left. + k\hat{x}_\alpha \int_S n_\beta \tilde{P}_{\alpha\beta}(\eta_\alpha, \omega_D) e^{-ik\eta_\alpha \hat{x}_\alpha} \, ds + \int_s \rho_0 n_\alpha \tilde{A}_\alpha(\eta_\alpha, \omega_D) e^{-ik\eta_\alpha \hat{x}_\alpha} \, ds \right\}. \tag{3.6}$$

Here, the integrands are all near-field quantities in the frequency domain calculated at the Doppler-shifted angular frequency ω_D, defined by

$$\omega_D = \omega D = \omega(1 - U_\alpha \hat{x}_\alpha/c), \tag{3.7}$$

with D being the Doppler factor. In deriving this, we have assumed that the velocity of the moving body is constant so that U_α is independent of the source time τ. This is

usually the case for airframe noise problems where the aircraft speed is approximately constant during the time interval at landing approach in which noise radiation is a concern.

Two features can be immediately seen from the result (3.6). The first is the far-field characteristics of the radiated sound, including the cylindrical spreading of the waves in the far field, indicated by the inverse square-root dependence of the pressure on $|x_\alpha|$ and the directivities associated with each of the three source types. The cylindrical spreading is a well-known feature of two-dimensional waves, but it not explicitly brought out in the original Ffowcs Williams/Hawkings equation, though that equation is in principle also valid for two-dimensional sources. The second is the absence of the retarded-time calculations in the integrals. Instead, the planar and contour integrals are calculated in the frequency domain with the proper Doppler shift in frequency. This is an advantage over the retarded-time formulation. Because the sampling of source time history does not usually coincide with the retarded time, the integration in the original Ffowcs Williams/Hawkings equation requires data interpolation, a very time-consuming but necessary step in that formulation. This is completely avoided here. It should also be pointed out that the extra calculations of the Fourier transformations in (3.6) for the near-field quantities are actually trivial. This is basically because numerical fast Fourier transform (FFT) is very efficient compared with other operations in the computation. Besides, in many situations, the spectral properties of the near-field quantities are of interest themselves so that near-field results in the frequency domain may be already available from the near-field modelling. In that case, there is no extra calculation in the far-field computation by (3.6).

As mentioned in previous sections, the original Ffowcs Williams/Hawkings equation is in principle valid for both three- and two-dimensional problems. It can be applied to two-dimensional problems provided that the source domains (the domains of integration) are regarded large in one direction to simulate the two-dimensional behaviour. Apart from the difficulty in explicitly bringing out the physics of the sources and their sound, that approach is also very inefficient. This is because the integration must be performed over a long range in that direction with an invariant source distribution but with variations due to the retarded-time calculation. Clearly, the result (3.6) not only avoids the retarded-time calculation, but also reduces all the integrals by one dimension, from spaces and surfaces respectively to planes and contours. This makes a difference in computational efficiency by orders of magnitude. Furthermore, the explicit two-dimensional result (3.6) also avoids the issue of convergence when applying the original Ffowcs Williams/Hawkings equation to two-dimensional problems. In that case, because the sources are invariant in one dimension and the three-dimensional Green function only provides a decay of the inverse distance, namely $1/|y_\alpha|$ at large $|y_\alpha|$, the convergence of the integrals in this direction critically depends on the variations of the sources with the retarded time. In that formulation, the convergence of the spatial integrals is achieved only if the sources decay sufficiently rapidly at large time.

The result (3.6) can also be normalized to explicitly reveal the functional dependence of the radiated sound on parameters such as the flow Mach number and the Doppler factor due to the source motions. To this end, we follow the convention of dimensional analysis by scaling the near-field quantities according to

$$\{T_{\alpha\beta}, P_{\alpha\beta}, A_\alpha\} \sim \{\rho_0 U^2, \rho_0 U^2, U^2/l\}, \tag{3.8}$$

where U is the typical value of the flow velocity and l the typical length scale of the

sources. With this, the three terms in the result (3.6) can all be normalized and the far-field pressure becomes

$$p(x_\alpha, t) = \rho_0 c^2 \left(\frac{l}{8\pi|x_\alpha|} \right)^{1/2} \left\{ \hat{x}_\alpha \hat{x}_\beta Q_{\alpha\beta} \frac{M^{7/2}}{D^{5/2}} + \hat{x}_\alpha F_\alpha \frac{M^{5/2}}{D^{3/2}} + S \frac{M^{3/2}}{D^{1/2}} \right\}, \qquad (3.9)$$

where three non-dimensional quantities $Q_{\alpha\beta}$, F_α and S are introduced for brevity. They are basically the three integrals in (3.6) normalized by (3.8), and thus can be regarded as the integrated source functions respectively for quadrupoles, dipoles and monopoles; they are all of the order of unity. This non-dimensional result brings out the physical features of the radiated sound. Apart from the cylindrical spreading and far-field directivities already analysed in (3.6), it also explicitly shows how the sound radiation depends on the flow Mach number M and the Doppler factor D. It is easy to summarize from (3.9) that

$$p \sim \frac{M^{(2n+3)/2}}{D^{(2n+1)/2}}, \qquad (3.10)$$

where $n = 0, 1, 2$ respectively for monopoles, dipoles and quadrupoles. Note that the Mach number dependence precisely recovers that discussed previously based on dimensional analysis (e.g. Ffowcs Williams 1969; Crighton 1975). The first term in the curly brackets in (3.9) also recovers the results derived in Ffowcs Williams & Hawkings (1968) for shallow-water waves generated by quadrupole sources (unsteady flows). In that paper, the approach of retarded-time integration is used to derive the wave field. It explicitly brings out the two-dimensional features of the shallow-water wave but is not very convenient for numerical computation because of the inverse square-root singularities in the integrand.

4. Near-field formulation for vortex/airfoil interaction

To demonstrate the application and numerical implementation of the two-dimensional version of the Ffowcs Williams/Hawkings equation, we choose to work with a Joukowski airfoil moving at constant velocity U in the negative x_1-direction and interacting with a concentrated vortex of constant strength. For sufficient low flow Mach number, the near-field flow can be approximated as incompressible. As illustrated in figure 1, the near field will be solved in the coordinate system fixed on the airfoil. The relation between the two coordinate systems is given by (2.9) in the previous section and is simply $x_1 = \eta_1 - Ut$ and $x_2 = \eta_2$. In this reference frame, the airfoil is embedded in a uniform flow of velocity U in the positive x_1-direction and subject to the incidence of an incoming vortex. The choice of the Joukowski airfoil, together with the incompressible assumption, enables us to solve the problem analytically by the conforming mapping

$$\eta = f(\zeta) = e^{-i\alpha} \left(\zeta + b - \zeta_e + \frac{b^2}{\zeta + b - \zeta_e} \right), \qquad (4.1)$$

which transforms the airfoil into a circle, where $\eta = \eta_1 + i\eta_2$ are the complex coordinates in the physical plane fixed on the airfoil and $\zeta = \zeta_1 + i\zeta_2$ are the transformed coordinates in the mapping plane. The angle of attack of the airfoil is denoted by α and the parameter b sets the origin of the coordinate system in relation to the trailing edge of the airfoil, as shown in figure 2. The quantity ζ_e is the point on the circle corresponding to the sharp trailing edge. It is given by
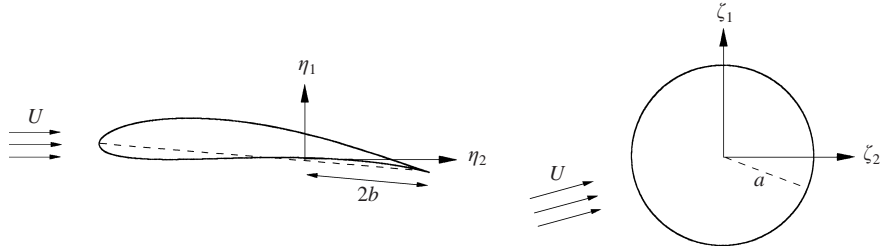
$$\zeta_e = (a^2 - h^2)^{1/2} - ih, \qquad (4.2)$$

FIGURE 2. A Joukowski airfoil in a uniform mean flow in the physical plane (η_1, η_2) and its conforming mapping to a circle in the mathematical plane (ζ_1, ζ_2). The mean flow directions in the two planes are different because of the non-zero angle of attack of the airfoil.

where a is the radius of the transformed circle and h is a parameter determining the shape and thickness of the airfoil.

The flow is disturbed by a vortex of constant strength Γ_0 whose trajectory is denoted by $\eta_0(t)$ in the complex physical plane and by $\zeta_0(t)$ in the mapping plane. Because of the incoming vortex, flow fluctuations are produced and the airfoil responds to these fluctuations by shedding vorticity from its trailing edge. The shed vorticity will also be represented by discrete vortices with strength $\Gamma_j(t)$ and trajectories $\eta_j(t)$ and $\zeta_j(t)$, respectively in the physical and mapping plane, where $j = 1, 2, \ldots N$, with N being the total number of vortices shed from the trailing edge. The strengths of the shed vortices vary with time and will be determined by the emendated Brown & Michael equation (Brown & Michael 1954; Howe 1996). The complex velocity potential W is simply given by the circular theorem in the mapping plane, namely

$$W(\zeta) = U\left(\zeta e^{-i\alpha} + \frac{a^2}{\zeta e^{-i\alpha}}\right) + \frac{\Gamma_c}{2\pi i}\ln\zeta + \frac{1}{2\pi i}\sum_{j=0}^{N}\Gamma_j\ln\frac{\zeta(\zeta - \zeta_j)}{a^2 - \zeta\zeta_j^*}, \qquad (4.3)$$

where Γ_c is the circulation around the airfoil and the asterisk indicates complex conjugate. The circulation around the airfoil is necessary to provide the airfoil with lift and to satisfy the Kutta condition at the sharp trailing edge. Clearly, the value of the circulation approaches that for steady flows when the incoming vortex is far from the airfoil, either at large negative or large positive time. That limiting value is given by the classic result

$$\Gamma_c(\pm\infty) = 4\pi a U \sin(\phi_e - \alpha), \qquad (4.4)$$

with ϕ_e being the argument of ζ_e defined by (4.2). Note that the change in the circulation of the airfoil must be balanced instantly by the shedding at the trailing edge so that we have

$$\mathrm{d}(\Gamma_N + \Gamma_c)/\mathrm{d}t = 0, \qquad (4.5)$$

where we have labelled the Nth vortex as the one that is still connected to the trailing edge. Those shed at previous times and having moved away from the edge do not have strength fluctuations, and hence do not appear in the time derivatives in (4.5). This equation can be integrated to yield

$$\Gamma = \Gamma_c + \sum_{j=0}^{N}\Gamma_j = \Gamma_0 + \Gamma_c(\pm\infty), \qquad (4.6)$$

which is basically the statement of vorticity conservation. Here, we have used Γ to denote the total vorticity in the flow, including that around the airfoil. Note that the

integration of (4.5) to yield the total vorticity (4.6) is done in a piecewise manner in time, because each of the shed vortices has a different time interval in which its strength varies with time. This is why the strengths of all the vortices are in the integrated conservation law, but only one appears in the differential form of this law (4.5), which represents an instantaneous relation.

From the complex potential (4.3), the flow velocity is simply given by

$$u_1 - iu_2 = \frac{dW}{d\eta} = \frac{1}{f'(\zeta)} \frac{dW}{d\zeta}, \tag{4.7}$$

where f' is written for $d\eta/d\zeta$ which can be easily found from (4.1) as

$$f'(\zeta) = e^{-i\alpha} \left(1 - \frac{b^2}{(\zeta + b - \zeta_e)^2} \right), \tag{4.8}$$

and the quantity $dW/d\zeta$ is given by (4.3) as

$$\frac{dW}{d\zeta} = U \left(e^{-i\alpha} - \frac{a^2}{\zeta^2 e^{-i\alpha}} \right) + \frac{\Gamma}{2\pi i\zeta} + \frac{1}{2\pi i} \sum_{j=0}^{N} \Gamma_j \left(\frac{1}{\zeta - \zeta_j} + \frac{\zeta_j^*}{a^2 - \zeta\zeta_j^*} \right). \tag{4.9}$$

The results (4.7) to (4.9) give the velocity in the flow except at the vortex locations when $\zeta \to \zeta_j$. At these locations, the velocity must be determined by the Roth rule that excludes the singular contributions from the vortex motions of the individual vortex itself. The regular part of the total velocity is the one with which the individual vortex moves. By denoting the velocity of the kth vortex by V_k, the mathematical form of the Roth rule reads

$$V_k = \lim_{\eta \to \eta_k} \left(\frac{dW}{d\eta} - \frac{\Gamma_k}{2\pi i} \frac{1}{\eta - \eta_k} \right) = \frac{1}{f'(\zeta_k)} \lim_{\eta \to \eta_k} \left(\frac{dW}{d\zeta} - \frac{\Gamma_k}{2\pi i} \frac{f'(\zeta)}{f(\zeta) - f(\zeta_k)} \right). \tag{4.10}$$

The last step follows from the use of (4.7) and (4.1). By carrying out the limiting operation, this result can be rewritten as

$$V_k = \frac{1}{f'(\zeta_k)} \left\{ U \left(e^{-i\alpha} - \frac{a^2}{\zeta^2 e^{-i\alpha}} \right) + \frac{\Gamma}{2\pi i\zeta} + \frac{1}{2\pi i} \sum_{j=0}^{N} \Gamma_j \left(\beta_{kj} + \frac{\zeta_j^*}{a^2 - \zeta_k\zeta_j^*} \right) \right\}, \tag{4.11}$$

where

$$\beta_{kj} = \begin{cases} (\zeta_k - \zeta_j)^{-1} & \text{for} \quad k \neq j \\ -0.5 f''(\zeta_k)/f'(\zeta_k) & \text{for} \quad k = j, \end{cases} \tag{4.12}$$

with f'' defined by

$$f''(\zeta) = \frac{d^2\eta}{d\zeta^2} = \frac{2e^{-i\alpha}b^2}{(\zeta + b - \zeta_e)^3}. \tag{4.13}$$

The above results specify the near-field flow in terms of the vortex strengths Γ_j and trajectories $\zeta(t)$ with $j = 0, 1, 2, \ldots N$. These quantities have to be determined by incorporating flow separation models in the formulation. This will be done through the emendated Brown & Michael equation (Brown & Michael 1954; Howe 1996).

In this model, the fully viscous process of flow separation in the local region close to the trailing edge of the airfoil is modelled as unsteady vorticity production in potential flow at the sharp edge, in the form of vortex shedding. The motions and the strength fluctuations of the shed vortices are governed by local dynamics and the rate of shedding is determined by the unsteady Kutta condition at the sharp edge that requires finite velocity at the edge. The physical reasoning and assumptions of

this model have been discussed previously in the literature and will not be repeated here. The only new part we introduce here is the mechanism by which the vortex breaks away from the trailing edge. At any time, the model assumes that a vortex is connected to the edge through a vortex sheet that feeds vorticity shed from the edge to the vortex core. The vortex core can also be regarded as the result of the vortex sheet roll-up. For the airfoil/vortex interaction problem, the flow fluctuations cause both positive and negative vortex shedding. The shed vorticity forms a distribution along the vortex sheet. The formation of discrete vortices results from the local evolution of the vortex sheet. We argue that the vortex sheet stretches most significantly at locations where the vorticity distribution changes sign. This provides a mechanism to implement the breakaway of the shed vortices from the edge. A vortex is connected to the edge and is fed with vorticity so that its strength varies monotonically with time until the rate of shedding becomes zero. At this time, the vortex breaks away and its strength will remain unchanged afterwards. The flow separation will be accounted for from that time by a new vortex. This way, the flow separation induces a series of vortices forming the airfoil wake.

By balancing the local momentum equation on the vortex sheet, as is done by Howe (1996), the equations for the motions of the vortices can be derived. Without repeating the procedure, we quote the equation as

$$\frac{\mathrm{d}\boldsymbol{x}_k}{\mathrm{d}t} \cdot \nabla \Psi_i + \frac{\Psi_i}{\Gamma_k} \frac{\mathrm{d}\Gamma_k}{\mathrm{d}t} = \boldsymbol{v}_k \cdot \nabla \Psi_i. \tag{4.14}$$

Here, $\boldsymbol{x}_k$ is the trajectory vector of the kth vortex with strength Γ_k, both being a function of time. The quantity Ψ_i is the stream function of the potential flow around the airfoil of zero circulation with unity velocity at infinity in the ith direction ($i = 1, 2$). The velocity $\boldsymbol{v}_k$ is the local flow velocity at the location of the kth vortex without the singular contribution from the vortex itself. It is given in (4.11) in complex form. Equation (4.14) is expressed in terms of quantities in the physical plane. To facilitate the incorporation of this model into the near-field formulation in terms of complex variables in the mapping plane, we convert (4.14) into complex variable format. This can be done by replacing $\boldsymbol{x}_k$ by η_k, $\boldsymbol{v}_k$ by V_k and Ψ_i by the imaginary part of its complex potential. Thus, (4.14) can be re-written as

$$\mathrm{Im}\left\{ \left(\frac{\mathrm{d}\eta_k}{\mathrm{d}t} - V_k^* \right) \frac{\mathrm{d}W_i}{\mathrm{d}\eta} + \frac{W_i}{\Gamma_k} \frac{\mathrm{d}\Gamma_k}{\mathrm{d}t} \right\} = 0, \tag{4.15}$$

where Im means the imaginary part of its argument and W_i is the complex potential around the airfoil of zero circulation with unity velocity at infinity in the ith direction ($i = 1, 2$). This result can be converted to a form without the imaginary sign Im by re-writing it in terms of the difference between the quantity in the curly bracket and its complex conjugate. Some straightforward algebra then leads to

$$\left\{ \left(\frac{\mathrm{d}\eta_k}{\mathrm{d}t} - V_k^* \right) \frac{\mathrm{d}W_i}{\mathrm{d}\eta} + \frac{W_i - W_i^*}{\Gamma_k} \frac{\mathrm{d}\Gamma_k}{\mathrm{d}t} \right\} \left(\frac{\mathrm{d}W_i^*}{\mathrm{d}\eta} \right)^{-1} = \left(\frac{\mathrm{d}\eta_k}{\mathrm{d}t} - V_k^* \right)^*. \tag{4.16}$$

This result is cast in such a way that the right-hand side is independent of W_i. Thus, when it is applied to $i = 1$ and $i = 2$, the left-hand sides of the two resulting equations should be equal, which leads to a single equation for $\mathrm{d}\eta_k/\mathrm{d}t$. By further noting that $\mathrm{d}\eta_k/\mathrm{d}t = f'(\zeta_k)\,\mathrm{d}\zeta_k/\mathrm{d}t$, we finally have

$$\frac{\mathrm{d}\zeta_k}{\mathrm{d}t} + \frac{B(\zeta_k)}{\Gamma_k} \frac{\mathrm{d}\Gamma_k}{\mathrm{d}t} = \frac{V_k^*}{f'(\zeta_k)}, \tag{4.17}$$

where B is determined by W_i and defined as

$$B(\zeta) = \left\{ \mathrm{Im}(W_1)\frac{\mathrm{d}W_2^*}{\mathrm{d}\zeta} - \mathrm{Im}(W_2)\frac{\mathrm{d}W_1^*}{\mathrm{d}\zeta} \right\} \Big/ \mathrm{Im}\left(\frac{\mathrm{d}W_1}{\mathrm{d}\zeta}\frac{\mathrm{d}W_2^*}{\mathrm{d}\zeta} \right) = \zeta\frac{|\zeta|^2 - a^2}{|\zeta|^2 + a^2}. \qquad (4.18)$$

Here, the last step follows from the use of the complex potential

$$W_1(\zeta) = \zeta\mathrm{e}^{-\mathrm{i}\alpha} + \frac{a^2}{\zeta\mathrm{e}^{-\mathrm{i}\alpha}} \quad \text{and} \quad W_2(\zeta) = -\mathrm{i}\zeta\mathrm{e}^{-\mathrm{i}\alpha} + \frac{\mathrm{i}a^2}{\zeta\mathrm{e}^{-\mathrm{i}\alpha}}. \qquad (4.19)$$

These are simply the complex potentials for the airfoil in steady flow without circulation.

To determine the vortex motions from (4.17), an extra condition must be specified for the vortex strengths, which also appear in (4.17) as unknowns. This is provided by the unsteady Kutta condition applied at the sharp trailing edge. The Kutta condition requires that the velocity at the edge should always be finite. It is clearly satisfied provided that $\mathrm{d}W/\mathrm{d}\zeta$, given by (4.9), vanishes at the edge. This leads to

$$\Gamma_0 + \sum_{j=0}^{N} \Gamma_j\frac{a^2 - |\zeta_j|^2}{|a^2 - \zeta_j\zeta_e^*|^2} = 0, \qquad (4.20)$$

where ζ_e is the point on the circle in the mapping plane corresponding to the sharp trailing edge in the physical plane, given by (4.2). This then establishes the relation between the strengths and the trajectories of the vortices. Note that the strength of the vortex that is still connected to the sharp edge varies with time.

5. Analysis of near-field results

The near-field flow can now be solved from the formulation in the previous section. For a given incoming vortex, (4.17) and (4.20) can be used to find the strengths Γ_j and trajectories of the vortices in the mapping plane, namely, $\zeta_j(t)$ with $j = 0, 1, 2, \ldots N$. The results can then be used to derive the vortex trajectories in the physical plane according to (4.1). In the numerical computations given in the following, we normalize all length quantities by the radius of the circle, a, in the mapping plane. The constant mean flow velocity U will be used as the reference velocity scale. Thus, the velocity potentials and the vortex strengths are all normalized by aU, and time by U/a. The time scale is set so that the incoming vortex crosses the η_2-axis at $t = 0$. Also, the airfoil is determined by setting $b = 0.9$ and $h = 0.1$, which lead to the airfoil shape shown in figure 2. The strength of the incoming vortex is chosen to be $\Gamma_0/aU = 0.1$ and the airfoil angle of attack α is set at $5°$.

Because of the fluctuations induced by the vortex motions, the airfoil experiences fluctuations in its circulation. This is shown in figure 3, which plots the non-dimensional circulation Γ_c/aU as a function of the non-dimensional time tU/a. At both large positive and negative time when the incoming vortex is far from the airfoil, the circulation approaches the value given by (4.4). When the vortex interacts with the airfoil at finite time, however, the circulation fluctuates with maximum of the same order as the strength of the incoming vortex. Figure 3 shows that the change in circulation is not monotonic, which, according to the analysis given in the previous section for the vortex shedding mechanism, implies that more than one vortex is shed from the airfoil. This is because the fluctuations in the airfoil circulation are balanced by the vorticity production at the trailing edge and changes in the slope of the circulation as a function of time mean changes in the sign of the shed vorticity.
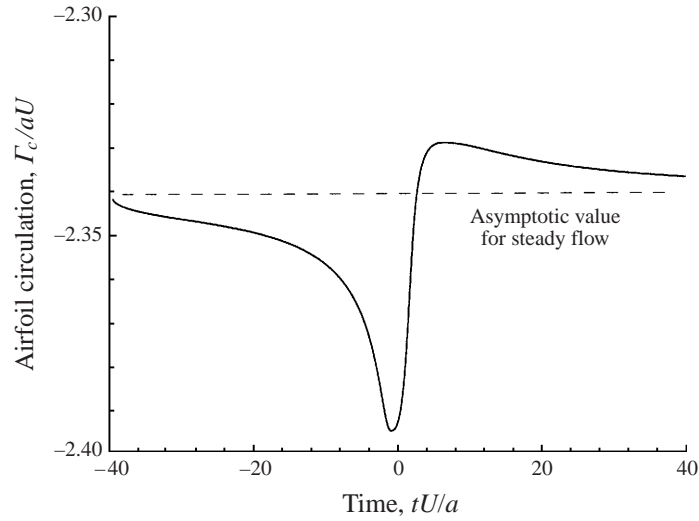
FIGURE 3. Fluctuations of the circulation around an airfoil at 5° of angle of attack and subject to the incidence of a vortex of strength $\Gamma_0/aU = 0.1$. The asymptotic value for steady flows is given by the large-time result of (4.4).
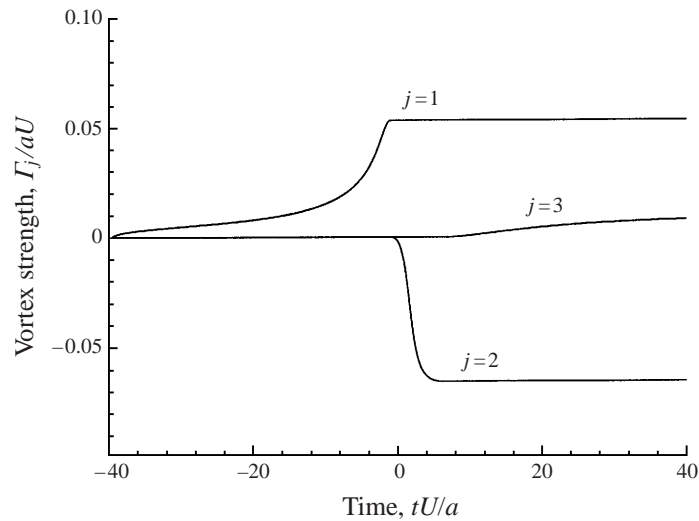

FIGURE 4. Strengths of the vortices shed from the airfoil trailing edge at 5° of angle of attack under the incidence of a vortex of strength $\Gamma_0/aU = 0.1$.

This is actually the mechanism we choose for the shed vortex to break away from the edge. According to this, figure 3 indicates that three vortices are shed from the edge. The vorticity accumulated in these three vortices is plotted in figure 4, in terms of the non-dimensional strength Γ_j/aU as a function of the non-dimensional time tU/a. As the incoming vortex approaches the airfoil, the airfoil experiences an upwash, leading to an increase in its lift. The increase in lift manifests itself as an increase in circulation in the negative direction, as shown in figure 3. This circulation change is balanced by the shedding of a positive vortex, plotted in figure 4. The strength of this first vortex grows with time until the incoming vortex passes the centre of the
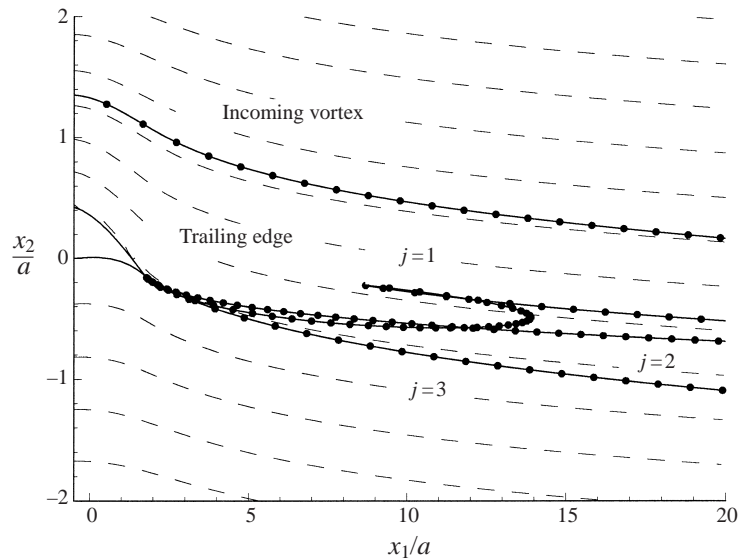
FIGURE 5. Trajectories of the vortices and the streamlines of the steady mean flow (the dashed curves). The dots on the trajectories indicate unity internals of the non-dimensional time tU/a.

airfoil and the airfoil lift starts to decrease. At this time, the first vortex breaks away from the trailing edge and becomes a free vortex in that its strength does not change any more. Also at this time, negative vorticity is shed, which is accumulated by the second vortex. Again, the strength of the second negative vortex grows with time until it reaches its maximum and its role in the flow separation modelling is taken over by the third vortex.

The trajectories of these three shed vortices are shown in figure 5. The dots on the trajectories indicate time intervals of 1 in terms of the non-dimensional time tU/a. It is interesting to note that the trajectories of the vortices are quite different from the streamlines of the base flow, also shown in figure 5 by the dashed curves. This is because the vortices are in fully nonlinear motion, jointly controlled by the convecting mean flow and the induced flow due to the vortices themselves. It is also these nonlinear motions that generate sound. As explained by the theory of vortex sound (Powell 1964; Howe 1975), vortices convecting at exactly the mean flow velocity are silent and sound is generated only when the vortices cross the streamlines of the mean flow.

From the strengths and trajectories of the vortices, all the quantities in the near-field flow can be found. Of particular interest for the sound generation is the pressure fluctuation on the airfoil surface. This can be easily found by making use of the Bernoulli equation, which reads

$$p_s + \frac{1}{2}\rho_0 \left| \frac{\mathrm{d}W}{\mathrm{d}\eta} \right|^2 + \rho_0 \,\mathrm{Re}\left(\frac{\mathrm{d}W}{\mathrm{d}t} \right) = p_\infty + \frac{1}{2}\rho_0 U^2, \tag{5.1}$$

where p_s and p_∞ are pressures respectively on the airfoil surface and at infinity and ρ_0 is the constant mean density. The symbol Re means the real part of its argument. From this, the surface pressure can be easily calculated, in terms of Γ_j and ζ_j, by

using the complex potential (4.3) and its derivative (4.9). Thus, we have

$$\left|\frac{\mathrm{d}W}{\mathrm{d}\eta}\right| = \frac{|\zeta - \zeta_e + b|^2}{2\pi a|(\zeta - \zeta_e + b)^2 - b^2|} \left|\Gamma - 4\pi U \operatorname{Im}(\zeta e^{-\mathrm{i}\alpha}) + \sum_{j=0}^{N} \Gamma_j \frac{a^2 - |\zeta_j|^2}{|\zeta - \zeta_j|^2}\right|, \qquad (5.2)$$

where ζ is now on the circle of radius a in the mapping plane, namely

$$\zeta = a \exp(\mathrm{i}\phi) \quad \text{with} \quad 0 \leqslant \phi < 2\pi. \qquad (5.3)$$

Similarly, the time derivative of the complex potential W can be found to be

$$\frac{\mathrm{d}W}{\mathrm{d}t} = \frac{2\phi_N - \phi}{2\pi} \frac{\mathrm{d}\Gamma_N}{\mathrm{d}t} - \frac{1}{\pi} \sum_{j=0}^{N} \Gamma_j \operatorname{Im} \frac{\mathrm{d}\zeta_j/\mathrm{d}t}{\zeta - \zeta_j}, \qquad (5.4)$$

where we have introduced ϕ_N to denote the argument of $\zeta - \zeta_N$.

It is very easy to implement the above results numerically to calculate the surface pressures on the airfoil. This can be done everywhere on the airfoil except at the sharp trailing edge, which, in the mapping plane, corresponds to the point $\zeta = \zeta_{e^\alpha}$. At this point, the first term on the right-hand side of (5.2) becomes infinite, but the second term vanishes so that the calculation must be done as a limiting process. To proceed with the limiting process, we rewrite (5.3) in the vicinity of the trailing-edge point, $\zeta_e = a \exp(\mathrm{i}\phi_e)$, as

$$\zeta = a \exp(\mathrm{i}\phi_e + \mathrm{i}\varepsilon) = \zeta_e(1 + \mathrm{i}\varepsilon) \quad \text{as} \quad \varepsilon \to 0. \qquad (5.5)$$

By substituting this into (5.2) and expanding the result in term of the vanishing parameter ε, it is straightforward to show that

$$\left|\frac{\mathrm{d}W}{\mathrm{d}\eta}\right| = \frac{b}{a^2} \left|aU \cos(\phi_e - \alpha) - \frac{1}{2\pi} \sum_{j=0}^{N} \Gamma_j \frac{a^2 - |\zeta_j|^2}{|\zeta_e - \zeta_j|^2} \operatorname{Im} \frac{\zeta_e}{\zeta_e - \zeta_j}\right| \qquad (5.6)$$

as $\varepsilon \to 0$, namely at the trailing edge of the airfoil, where ϕ_e is the argument of ζ_e and α is the angle of attack of the airfoil. Clearly, this result is always finite, which leads to finite pressure at the sharp trailing edge, as guaranteed by the Kutta condition.

It should be noted that the surface pressures do not approach the pressure at infinity at large times, both positive and negative. This is because the airfoil experiences a lift in steady flows, which is the large time limit when the incoming vortex is far away from the airfoil. For acoustic computation, it is the pressure fluctuations that are important. Thus, we will calculate the fluctuations according to the definition

$$\Delta p_s = p_s(x_\alpha, t) - p_s(x_\alpha, t \to \infty), \qquad (5.7)$$

and normalize the results by the dynamic head of the mean flow, namely

$$q = \tfrac{1}{2} \rho_0 U^2. \qquad (5.8)$$

Some examples of the surface pressures are plotted in figure 6 for the non-dimensional pressure as a function of the non-dimensional time. The most significant pressure fluctuations are seen in the region close to the leading edge of the airfoil when the incident vortex interacts with it. The incident vortex also interacts with the trailing edge, but the shedding of vorticity at the edge reduces that interaction so that the induced pressure fluctuations are less intense. This has been discussed previously (Howe 1976; Amiet 1990) and is known to be the reason for the complete silence, predicted by linear theories, when a vortex passes a trailing edge with exactly the same velocity as the mean flow with shed vortices convecting also at that velocity.
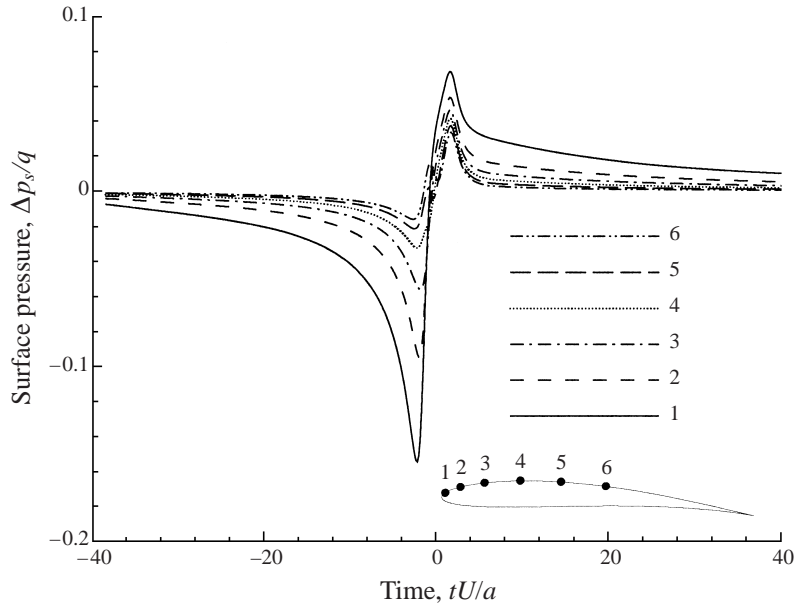
FIGURE 6. Pressure fluctuations on the airfoil surface at selected locations. The airfoil is at 5° of angle of attack and the incident vortex is of strength $\Gamma_0/aU = 0$.

6. Far-field computation

For low Mach number flows with rigid bodies in motion, the dominant sound is given by the dipole term due to surface stresses in (3.6). An example of this application is the case of airframe noise in which the typical flow Mach number is about 0.2 and the components of the high-life systems can be regarded as rigid at frequencies of interest to aircraft noise certification. Furthermore, viscous effects are usually negligible so that the surface stresses reduce to surface pressures. Thus, the sound in the far field is simply given by

$$\tilde{p}(x_\alpha, \omega) = e^{ik|x_\alpha|} \left(\frac{k}{8i\pi|x_\alpha|} \right)^{1/2} \int_s \hat{x}_\alpha n_\alpha \Delta \tilde{p}_x(\eta_\alpha, \omega_D) e^{-ik\eta_\alpha \hat{x}_\alpha} \, ds. \tag{6.1}$$

With the surface pressure fluctuations given, such as those computed in the previous section for the vortex/airfoil interaction, the far-field radiation can be easily calculated from this result. This simply involves converting the surface pressure fluctuations in a time domain to surface pressure spectra in a frequency domain and integrating the results over the two-dimensional body. The results are basically the far-field pressure spectra and the far-field pressure fluctuations can then be easily derived by a simple Fourier transformation.

By following this procedure and using the surface pressure fluctuations derived in the previous section, some examples of the far-field pressure fluctuations from the vortex/airfoil interactions are shown in figure 7. The results are plotted in terms of the non-dimensional pressure

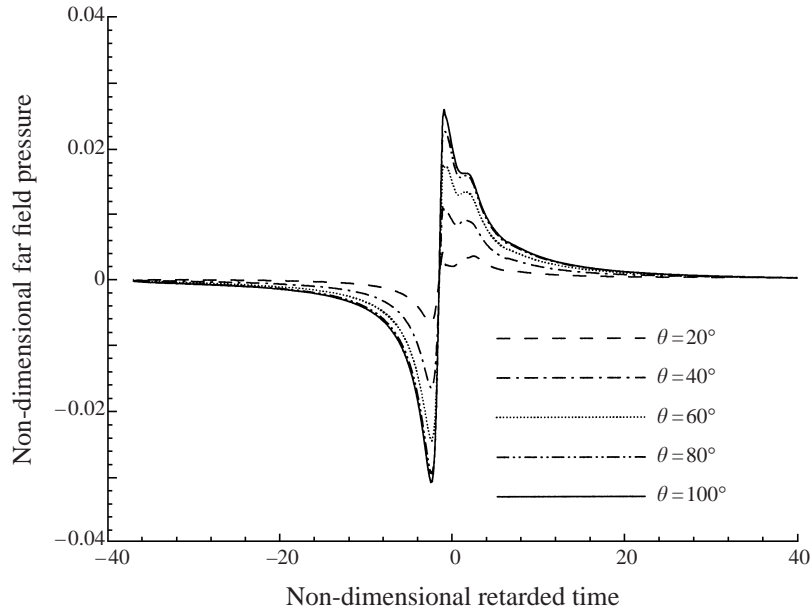$$\frac{p(x_\alpha, t)}{q} \left(\frac{|x_\alpha|}{a} \right)^{1/2} \frac{D^{3/2}}{M^{1/2}}, \tag{6.2}$$

FIGURE 7. Far-field pressure fluctuations at different angles distance $100a$ away from the airfoil. The non-dimensional pressure is defined by (6.2) and the non-dimensional retarded time by (6.3).

as a function of the non-dimensional retarded time

$$\frac{U}{aD}(t - |x_\alpha|/c), \qquad (6.3)$$

where q and D are defined respectively by (5.8) and (3.7). The far-field directivity angle θ in this figure is defined by

$$x_1 = |x_\alpha|\cos\theta \quad \text{and} \quad x_2 = |x_\alpha|\sin\theta. \qquad (6.4)$$

In calculating the results shown in figure 7, the far-field distance is taken to be $|x_\alpha| = 100a$ and the Mach number to be $M = 0.1$. The far-field pressure fluctuations basically show a pulse-like feature, having significant amplitude only when the incoming vortex is close to the airfoil with significant interactions. The pulse-like shapes are also very similar to those for the surface pressure fluctuations shown in figure 6.

The far-field radiation is relatively weak in the upstream and downstream directions. This can be seen from figure 7 and is more clearly demonstrated in figure 8 in terms of the directivity pattern of the non-dimensional radiated power. It is defined by

$$\frac{|x_\alpha|}{a}\frac{D^3}{M}\frac{1}{q^2}\int_t p^2(x_\alpha, t)\,\mathrm{d}t, \qquad (6.5)$$

and plotted in polar form. The far-field power shows typical dipole directivity, as is expected. However, the dipole axis is perpendicular neither to the airfoil chord nor to the mean flow. This is probably because the most significant radiation comes from the interactions between the vortex and the part of the airfoil close to the leading edge, as is seen in the surface pressure fluctuations analysed in the previous section. The unsteady forces furnished by these interactions are not necessarily normal to either the airfoil chord or the mean flow. Instead, the local airfoil geometry and
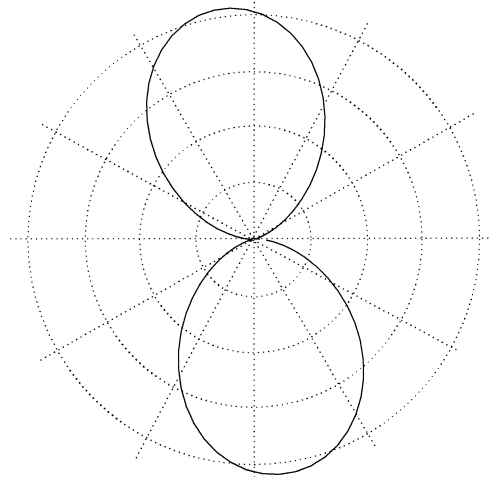
FIGURE 8. Directivity pattern of the far-field radiation at distance $100a$ away from the airfoil. The non-dimensional amplitudes are defined by (6.5).

the location of the incoming vortex determine these forces, and thus, the maximum radiation directions in the far field.

7. Conclusions

In this paper, we have derived a version of the Ffowcs Williams/Hawkings equation for computing far-field sound due to sources (moving body or flow) that can be approximated as two-dimensional. This has been shown to be much more efficient than applying the three-dimensional version to two-dimensional problems. Furthermore, the two-dimensional version has been shown to explicitly bring out the unique features of the far-field radiation associated with two-dimensional sources, which can provide guidelines for understanding and interpreting physical mechanisms in engineering applications.

A typical example is the noise from the leading-edge slats of aircraft high-lift systems. The spanwise dimensions of the slats are usually much larger than other dimensions (chord and thickness) so that the sources can be regarded as two-dimensional. In this case, the dominant contribution comes from the dipole term due to surface pressure fluctuations: the quadrupole contributions can be neglected due to their weakness and the monopoles are identically zero for rigid surfaces. This may explain the fact that airframe noise intensity scales on the flow Mach number according to the 5th power law in the middle frequency domain centred at about 1000 Hz (Sen *et al.* 1997; Guo *et al.* 1999). This explanation, however, has not always been apparent, because the 5th power law coincides with the prediction of sound scattered from turbulent flows by a sharp edge (Ffowcs Williams & Hall 1970). Because of this, airframe noise has been attributed to the sharp trailing edges of the wings (e.g. Bauer & Munson 1978; Fink 1979). While this may explain airframe noise from clean wing configurations when the high lift systems are not deployed (Crighton 1991), it is not supported by recent test data (Sen *et al.* 1997; Guo *et al.* 1999). The data show that airframe noise in the middle frequency domain is dominantly generated in the slat region, probably due to flow separation in the cove region of the slats (Guo 1997), instead of the trailing edges of the wings. In this case, the 5th power law is more

likely to be associated with the two-dimensional nature of the sources, rather than the sharp edge scattering. The sharp edges of the slats, namely their cusps and trailing edges, are in a relatively 'clean' flow without intense turbulence fluctuations. Thus, the scattering, if any, would be relatively weak because according to the theory by Ffowcs Williams & Hall (1970), strong scattering occurs only when intense turbulence fluctuations exist in a region close to the sharp edges within a typical wavelength.

Also important to note is that the 5th power law from sharp-edge scattering results from the assumption of potential flow at the edge where the flow becomes singular. If the flow is regular at the sharp edge, as commonly implied when the Kutta condition is applied, the scattered noise would not follow the 5th power law, which is also explicitly pointed out in Ffowcs Williams & Hall (1970). All these indicate that the experimentally observed 5th power law of the middle frequency component in airframe noise may be more satisfactorily understood by the two-dimensional nature of the sources associated with the flow in the slat region, even without any sharp-edge scattering.

REFERENCES

AMIET, R. K. 1976 Noise due to turbulent flow past a trailing edge. *J. Sound Vib.* **47**, 387–393.

AMIET, R. K. 1990 Gust response for flat-plate airfoils and the Kutta condition. *AIAA J.* **28**, 1718–1727.

BAUER, A. B. & MUNSON, A. G. 1978 Airframe noise of the DC-9-31. *NASA Contract Rep.* 3027.

BROWN, C. E. & MICHAEL, W. H. 1954 Effect of leading edge separation on the lift of a delta wing. *J. Aero. Sci.* **21**, 690–706.

BROOKS, T. F. & HODGSON, T. H. 1981 Trailing edge noise prediction from measured surface pressures. *J. Sound Vib.* **78**, 69–117.

CRIGHTON, D. G. 1975 Basic principles of aerodynamic noise generation. *Prog. Aerospace Sci.* **16**, 31–96.

CRIGHTON, D. G. 1981 Acoustics as branch of fluid mechanics. *J. Fluid Mech.* **106**, 261–298.

CRIGHTON, D. G. 1985 The Kutta condition in unsteady flow. *Ann. Rev. Fluid Mech.* **17**, 411–445.

CRIGHTON, D. G. 1991 Airframe noise. In *Aeroacoustics of Flight Vehicles: Theory and Practice* (ed. H. H. Hubbard). NASA Reference Publication 1258.

FFOWCS WILLIAMS, J. E. 1969 Hydrodynamic noise. *Ann Rev. Fluid Mech.* **1**, 197–222.

FFOWCS WILLIAMS, J. E. & HALL, L. H. 1970 Aerodynamic sound generation by turbulent flow in the vicinity of a scattering half plane. *J. Fluid Mech.* **40**, 657–670.

FFOWCS WILLIAMS, J. E. & HAWKINGS, D. L. 1968 Shallow water wave generation by unsteady flow. *J. Fluid Mech.* **31**, 779–788.

FFOWCS WILLIAMS, J. E. & HAWKINGS, D. L. 1969 Sound generation by turbulence and surfaces in arbitrary motion. *Phil. Trans. R. Soc. Lond.* A **264**, 321.

FINK, M. R. 1979 Noise component method for airframe noise. *J. Aircraft* **16**, 659–665.

GUO, Y. P. 1997 A model for slat noise generation. *AIAA Paper* 97-1647.

GUO, Y. P. 1999 Prediction of flap edge noise. *AIAA Paper* 99-1804.

GUO, Y. P., JOSHI, M. C., BENT, B. & YAMAMOTO, K. J. 1999 Noise characteristics of aircraft high lift systems. *J. Fluid Mech.* (Submitted).

HARDIN, J. C. 1980 Noise radiation from the side edge of flaps. *AIAA J.* **18**, 549–552.

HOWE, M. S. 1975 Contributions to the theory of aerodynamic sound, with application to excess jet noise and the theory of flute. *J. Fluid Mech.* **71**, 625–673.

HOWE, M. S. 1976 The influence of vortex shedding on the generation of sound by convected turbulence. *J. Fluid Mech.* **76**, 711–740.

HOWE, M. S. 1978 A review of the theory of trailing edge noise. *J. Sound Vib.* **61**, 437–465.

HOWE, M. S. 1996 Emendation of the Brown & Michael equation, with application to sound generation by vortex motion near a half-plane. *J. Fluid Mech.* **329**, 89–102.

LIGHTHILL, M. J. 1952 On sound generated aerodynamically I. General theory. *Proc. R. Soc. Lond.* A **211**, 564–587.

POWELL, A. 1964 Theory of vortex sound. *J. Acoust. Soc. Am.* **36**, 177–195.

SEN, R. 1996 Local dynamics and acoustics in a simple 2D model of airfoil lateral-edge noise. *AIAA Paper* 96-1673.

SEN, R., BLACKNER, A., YEE, P. & STOCKER, R. 1997 Airframe noise generation and radiation. *NASA Contract NAS*1-20090.